Non-contact detection of trench quality by UAV-LiDAR system

Wen Xiao
College of Engineering
Nanjing Agricultural University
Jiangsu Nanjing, China
WenX@stu.njau.edu.cn

Heqing Li
College of Engineering
Nanjing Agricultural University
Jiangsu Nanjing, China
hqli@seu.edu.cn

Deying Liu
College of Engineering
Nanjing Agricultural University
Jiangsu Nanjing, China
dyliu@njau.edu.cn

Yi Zuo
College of Engineering
Nanjing Agricultural University
Jiangsu Nanjing, China
yizuonjau@163.com

Wei Zhu
College of Engineering
Nanjing Agricultural University
Jiangsu Nanjing, China
15895192169@163.com

Yuning Yin
College of Engineering
Nanjing Agricultural University
Jiangsu Nanjing, China
yinyuning1998@163.com

***Abstract*—In order to promote the innovation of agricultural science and technology and the development of smart agriculture, a non-contact trench quality inspection system, UAV-LiDAR, is developed in this paper. The system uses the unmanned aerial vehicle (UAV) as the mobile flight platform, which can realize the non-contact trench quality data acquisition and automatic evaluation of the trench quality by carrying LiDAR, IMU, router and microcomputer. First of all, point cloud data sets of different areas of the whole farmland were acquired by UAV-LiDAR. Secondly. according to the normal deviation matching algorithm, appropriate frames were chosen to match the point cloud data of furrows in different regions, and the point clouds of each region were registered to the unified coordinate system to obtain the complete point cloud data of the whole farmland furrows. In the endusing the poisson surface reconstruction to realize the reconstruction surface of the complete furrow point cloudmeasuring the trench surface width, trench bottom width and trench depth of the furrow. The experimental results showed that the method proposed in this paper can effectively detect the working performance of the ditching machine. Compared with the manual measurement results, the identification time reduced by 15 $\sim$ 20 minutes, and the detection efficiency and accuracy are improved by 50% $\sim$ 66.67% and 22.96% $\sim$ 29.37%, respectively. It realizes the visual remote appraisal of the performance of the trench machine, and provides an intelligent appraisal means for the performance of agricultural machinery.**

***Index Terms*—the trench machine, identify the performance, UAV-LiDAR**

I. Introduction

Farmland trenching is an important part of agricultural activities, which can effectively regulate the circulation of water, fertilizer and heat in the whole farmland, and is conducive to improving the soil environment and improving the yield and quality of crops. Ditching can loosen the soil, promote the growth and development of crop roots, improve the utilization rate of water, promote fertilizer absorption, and enhance the resistance of crops.

To improve the efficiency of ditching, ditching machine has become an indispensable operating machinery. The ditching machine is mainly composed of trenching component, trench depth control system, power transmission component, soil retaining plate and spiral blades, etc. The working principle is as follows: the power transmission component transmits the power to the trenching component, the trenching component excavates the trench, the trench depth control system is responsible for regulating the trench depth, and the soil retaining plate and spiral blades cooperate to send the soil out of the furrow.

In recent years, the domestic and foreign scholars have carried out relevant research on the structure and performance of ditching machine. S. Senthilgavaskar invented an all-in-one ditching and ridging machine by using solar energy. The new machine uses free solar energy, which is cost-effective and low-cost, and suitable for small-scale agricultural activities [1]. Changho Yun et al. proposed stereovision-based guidance-line-extraction algorithm, and designed an automatic ridging and ditching tillage machine based on this algorithm. The classification accuracy of furrows and ridges can reach 90%, and the performance on flat land is no different from that of manual driving [2]. The driving path on the slope is similar to manual driving, with a slight deviation. According to the torque and energy characteristics, M.A. Matin and J. M. Fielke optimized the blade of the ditching machine, and studied the blade geometry (conventionalhalf-width and straight) , and compared the average power, peak power and specific energy to determine the performance of a certain blade at a specific speed. The experimental results showed that when the rotating speed is 500 RPM, the straight blade can save 20% $\sim$ 25% power compared with the conventional blade and the half-width blade. When the speed is 375 RPM, straight blades are still very efficient [3].

In addition to studying the structure and performance of the ditching machine, it is also essential to test the performance of the ditching machine. The traditional testing method is that the detection personnel select one measurement point at an

978-1-6654-9291-1/22/$31.00 © 2022 IEEE

average interval of 2 m in the detection area with a length of no less than 20 m. At least 10 measuring points are chosen for each furrow, and the furrow surface width, furrow bottom width and furrow depth are measured with a tape measure. In order to reduce the measurement error, the detection personnel will manually rectify the measurement value and calculate the average value and standard deviation of the trench depth, width of the trench surface and width of the trench bottom. This detection method has low efficiency, and there are human factors in the detection data, which can not meet the current requirements of identification. Therefore, the researchers have put forward their own detection methods. M.A. Matin studied the performance of the blade of the ditching machine, compared the average power, peak power and specific energy, to judge the performance of the ditching machine [3]. Y. Wang and W. Xue et al. proposed the study of DEM and soil bin of biomimetic disc furrow opener, analyzed the resistance of BCDFOs furrow opener by discrete element method, and evaluated soil disturbance characteristics by calculating soil expansion rate and disturbance coefficient [4]. In 2018, C. Yun and H. J. Kim proposed a stereo-vision guidance-line detection system applied in furrow planting field to detect the deviation degree of autonomous tractor's automatic navigation in the furrow, and accurately locate the position of the tractor in the field [5].

In this paper, we proposed a non-contact detection of trench quality by UAV-LiDAR system and developed to remotely detect the furrow performance of trench machine. The system could remotely acquire the whole farmland information, register the data of 2×2 areas to obtain a complete farmland model, detect the parameter information of the trench, and input the operation performance test parameters of the trench machine into the three-dimensional point cloud agricultural machinery performance test platform.

II. Materials and Methods

A. Data acquisition equipment

In this paper, as the experimental site is farmland, the field environment is complicated, which affects the accuracy of data acquisition, so we choose the 16 channels 3D LiDAR VLP-16 produced by Velodyne Company. This LiDAR has high accuracy (± 3 cm), can adapt to the harsh environment, and is small in size and light in weight (about 1 kg), which is easy to carry. It has become an ideal type of UAV carrying [6]–[8]. The data acquisition frequency is 10 Hz and speed is 300,000 points per second. LiDAR has a wide range of applications, for example, the mapping of tree crowns [9], map reconstruction and Vehicle obstacle avoidance [10], gully-erosion estimation and terrain reconstruction [11]. However, the shaking of UAV in flight makes the data produce angle deviation, so a 9-axis AHRS inertial navigation calibration point cloud data is required. The AHRS of Xsens MTi-300 can output three-axis attitude angles, which can enrich LiDAR point cloud data. The Ethernet switch is used to expand the physical interface of mobile workstation and connect the communication of external devices. Since the data size is related to the acquisition time, about 1 G per minute, and the collection time is 5 $\sim$ 8 minutes, a mirco-host with large memory is required. The micro-host chooses 16 G memory /256 G solid state, and installs Ubuntu 16.04 operating system to save point cloud data. The battery is responsible for supplying power to the acquisition equipment, the power requirement of the acquisition equipment is between 5 $\sim$ 20 V. The output voltage / current of the battery is 22.6 V / 10 A, which meets the voltage and current requirements of the acquisition equipment. The total weight of the data acquisition equipment is 3.5 kg. Taking the payload of the UAV into account, the UAV selects DJI M600 Pro, with the maximum load capacity of 5 kg and the endurance of 18 minutes, which can ensure the complete collection of data. Table I lists the specific models and parameters of the devices. The data acquisition device is shown in the Fig. 1, and the frame of the data acquisition device is shown in the Fig. 2.

Fig. 1. Data acquisition equipment

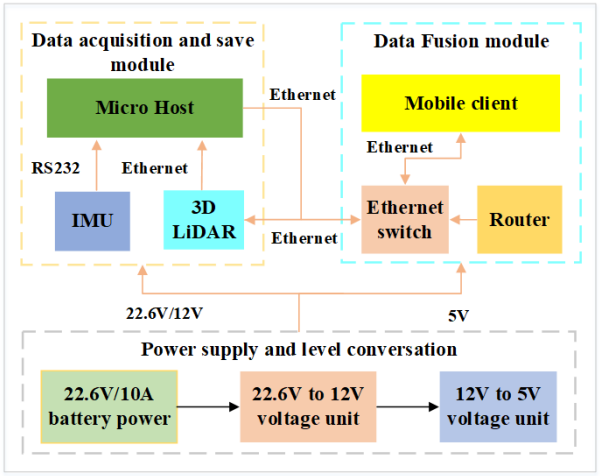

Fig. 2. Framework of data acquisition equipment

B. Field data collection

The MAE and RMSE of the 3D LiDAR ranged from 0.003 $\sim$ 0.007 m and 0.004 $\sim$ 0.098 m, respectively at the distances 1 $\sim$ 5 m between the LiDAR and the object. Therefore, the

TABLE I
SPECIFIC MODELS AND PARAMETERS OF THE DEVICES.

Sensor	Models	Parameters
UAV	DJI M600 Pro	Dimension: 1668 mm × 1518 mm × 727 mm Load: 5 kg Hover precision: Vertical (± 0.5 m) Horizontal (± 1.5 m) Time of flight: 18 minutes
3D Lidar	VLP-16 (Velodyne)	16 Channels Range Accuracy: ± 3 cm (Typical) Field Of View(Horizontal): 360° Field Of View(Vertical): +10° to -10° Measurement Range: 100 m Power requirements(VDC): 9 to 32 Weight(g): 1 kg
IMU	MTI-300 (Xsens)	Roll (RMS):0.2°(Static),0.3°(Dynamic) Pitch (RMS):0.2°(Static),0.3°(Dynamic) Yaw (RMS): 1.0°
Ethernet Switch Router	Mercury	Power requirements(VDC, A): 5, 0.6 type: S105C Power requirements(VDC): 5
Micro Host	GIGABYTE GB-BRi5H	Power requirements(VDC, A): 19, 3.42 Processor: intel i5 Memory: 8G Solid state drives: 256G Weight(kg): 1 kg

sensor has adequate accuracy for furrow measurement in the field, because the LiDAR is placed within 2 ∼ 3 m of the furrow.

The testing site was located in Yayuan Family Farm, Yangzhou City, Jiangsu Province, China. The testing site was divided into 2 × 2 areas, each area was 5 × 25 m, and each area had at least two trenches. The data acquisition was implemented in June 2020. The model number and parameters of the trenching machine are shown in the Table II . According to the local agronomic requirements, the standard trenching parameters settings are as below: Trenching type: trapezoid; Trench surface width: 20 cm; Trench bottom width: 15 cm; Trench depth: 25 cm. The UAV equipped with data acquisition equipment was manually operated to acquire data. The UAV used DJI M600 pro. The flying height of the UAV was 2 m, the flying speed was 1 m/s. The trenching scene of ditching machine as shown in the Fig. 3.

TABLE II
TRENCHING MACHINE SPECIFICATION.

Item	Unit	Design value
Mechanical type		Trench machine
Model number		1K-33
Structure type		Single disc type
External dimensions	mm	1400 × 930 × 1340
Rated power	kW	≥ 55.1
Power take-off speed	r/min	540
Operating speed range	m/s	0.7 ∼ 1
Trenching type		trapezoid
Trench depth	cm	15 ∼ 33
Trench surface width	cm	20 ± 2
Trench bottom width	cm	15 ± 2

Fig. 3. The trenching site of ditching machine

C. Data pre-processing and surface reconstruction

Trenching quality detection system of the overall data processing flow, as shown in Fig. 4. The detailed steps are as follows.

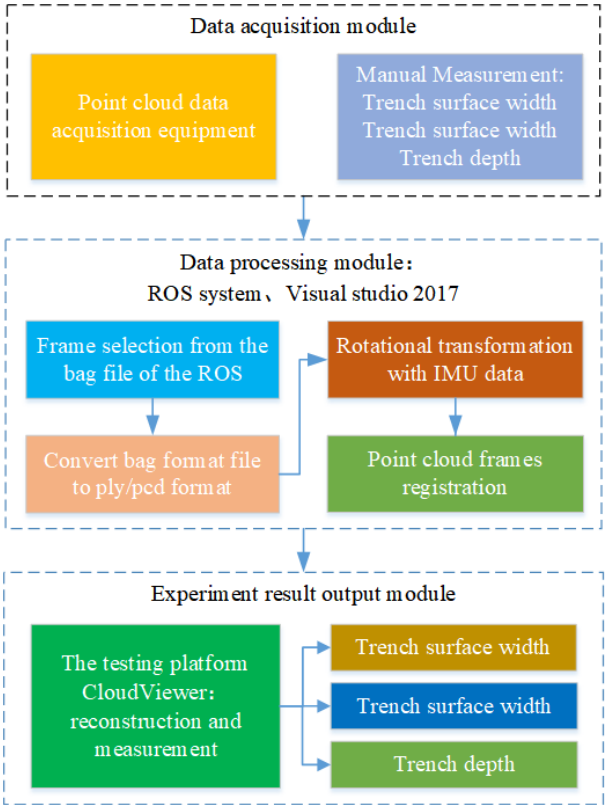

Fig. 4. Trenching quality detection system of the overall data processing flow

1) Data pre-processing: Data pre-processing includes point cloud frame data registration to each furrow reconstruction. The best way to operate LiDAR is to scan the scene while

the sensor remains static. However, in order to cover an entire field, the LiDAR needs to be moved to scan, so the position and attitude of the sensors need to be taken into account. Resulting data can be converted into a single frame, and then point cloud data can be generated through point cloud registration. Ideally multiple frames of data need to be used. The following paragraphs explain the steps for point cloud registration to generate point cloud data.

In the ROS system, the data of LiDAR and IMU are stored in two "bag" files respectively. The "bag" file is visualized in the Rviz interface, and the "bag" file of LiDAR is converted into "PLY/ PCD" format to select the appropriate frame for point cloud registration.

The point cloud registration method registers the point cloud data from the local coordinate system to the global coordinate system. Image registration is the core problem of 3D SLAM. Therefore, most researchers tend to study the iterative closest point method [12], [13]. Common registration algorithms include FPFH, Scan registration, ordinary NDT, NDT-ICP registration algorithm, SAC-IA-NDT and SAC-IA-ICP [14]–[16].

This paper proposes a registration algorithm based on normal deviation point matching [17]. The algorithm calculates the normal of the k-neighborhood and the angular deviation of the normal of the input point cloud related to the query point, with two steps :

(1) k-neighborhood search, KNN;

(2) Angle search. The pseudo-algorithm is shown in Algorithm 1.

Algorithm 1 Matching by normal deviation procedure

Require: kNNsearch is k nearest neighbour search algorithm. Q^k is the set of k nearest points to $\mathbf{p}_i$, $\mathbf{n}_{pi}$ and $\mathbf{n}_{qk}$ are the normal vectors associated with $\mathbf{p}_i$ and $\mathbf{q}_k$, respectively. θ_k is the angular deviation of the normal $\mathbf{n}_{qk}$ to the normal $\mathbf{n}_{pi}$. The threshold angle θ_t is watchdog to avoid matching of points with normals too far apart. The value of the threshold θ_t is the 40° and it is obtained by trial and error.

Ensure: $\mathbf{p}_i$,$\mathbf{q}_j$ is the correspondence of the query point $\mathbf{p}_i$ on the input point cloud P^N with a point $\mathbf{q}_j$ on the reference point cloud Q^M.

```
k ← 10
for all p_i ∈ P^N do
    Q^k ← kNNsearch(p_i, Q^M, k)
    for all q_k ∈ Q^k do
        θ_k ← cos^{-1}(n_qk, n_pi)
    end for
    θ_j ← min(θ_1,...,θ_k)
    if θ_j > θ_t then
        q_j ← q_1 (Nearest neighbour)
    end if
    p_i, q_j ← matching
end for
```

2) Surface reconstruction: The point cloud data registered was opened in the software CloudCompare, and extracted the furrow to be measured. The furrow to be measured was opened in the 3D point cloud agricultural machinery testing platform CloudViewer, and the trench model was reconstructed.

The trench bottom width, trench surface width and trench depth were extracted from the point cloud data. The testing platform CloudViewer was chosen to verify whether the studying results and accurary met the requirements. The testing platform CloudViewer used Poisson reconstruction algorithm to reconstruct the furrow model, which is one of the implicit surface reconstruction algorithms. Implicit surface reconstruction is to express the surface by implicit function, and to approximate the sampled 3D point cloud data by calculating the zero isosurface of implicit function. Usually, the RBF function interpolation method is adopted as the radial basis function to construct the implicit function, then the point cloud data is fitted, and finally the Zero Level Set of the implicit function is extracted. Classical implicit modeling algorithms include Poisson surface reconstruction, Loop subdivision surface reconstruction and Multi-level Partition Unity Implicit (MPU) and so on [18]–[21].

This paper proposed a novel Poisson algorithm based on normal deviation registration [22]. The Poisson surface reconstruction methods are motivated by calculating the characteristic function with surface boundary. The integral relationship between the sampling point and the indicator function is obtained from the gradient relationship of the surface. According to the integral relationship, the vector field of the point set is obtained by using the method of partition, and the approximation of the gradient field of the indicator function is calculated to form the Poisson equation. The approximate solution of Poisson equation is obtained by matrix iteration, the isosurface is extracted by moving cube algorithm, and the measured object model is reconstructed from the measured data point set. The trench poisson reconstruction as shown in Fig. 5.

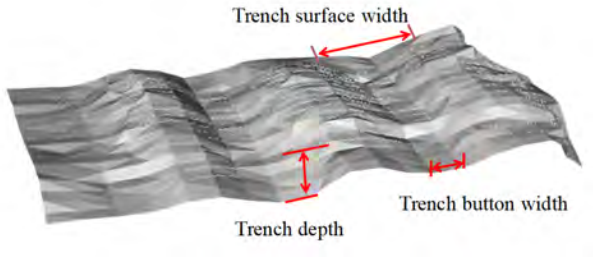

Fig. 5. Trench poisson reconstruction

Trench depth H from the highest point of the trench surface to the lowest point of the trench bottom, the calculation method is shown in Equation (1):

$$H = |y_{max} - y_{min}|, \tag{1}$$

y is the y-coordinate value;

TABLE III
MEASUREMENT DATA COMPARISON

Number	Reconstruction Measurement (cm)			Manual Measurement (cm)		
	Trench surface width	Trench bottom width	Trench depth	Trench surface width	Trench bottom width	Trench depth
1	20.87	16.43	23.93	21.5	16.0	23.5
2	21.26	15.94	24.47	22.0	16.5	25.0
3	20.45	15.81	22.87	21.0	15.5	22.0
4	21.76	13.44	23.26	22.0	14.0	22.0
5	21.27	14.62	24.72	21.0	15.0	22.5
6	21.09	15.47	23.35	21.5	16.0	24.0
7	20.43	15.76	23.16	21.0	16.5	23.5
8	21.13	16.79	23.78	21.0	17.0	23.0
9	21.61	16.91	23.67	21.5	17.5	23.5
10	20.53	17.08	25.49	21.0	17.5	25.0

Flight altitude: 2 $\sim$ 4 m; Flight speed: 2 m/s

TABLE IV
AVERAGE VALUE AND STANDARD VALUE COMPARISON

Value	Reconstruction Measurement (cm)			Manual Measurement (cm)		
	Trench surface width	Trench bottom width	Trench depth	Trench surface width	Trench bottom width	Trench depth
Average	21.04	15.825	23.87	21.35	16.15	23.4
Standard	20.0	15.0	25.0	20.0	15.0	25.0
Deviation	**1.04**	**0.825**	**-1.13**	1.35	1.15	-1.6

The UAV-LiDAR data acquisition time: 7 $\sim$ 10 minutes; Manual measurement time : 20 $\sim$ 30 minutes

Trench width W is calculated as shown in Equation (2):

$$W = |x_{max} - x_{min}|, \tag{2}$$

x is the x-coordinate value.

III. EXPERIMENT AND RESULT ANALYSIS

A. Experimental environment

All experiments in this paper were operated on a laptop computer (operating system: Windows 10 $\times$ 64, processor: Intel(R) Xeon(R) E-2176M, CPU: I5-6300HQ, graphics card: GeForce GTX950M). Visual Studio 2017 is the software platform for point cloud registration, and Point Cloud Library (PCL) was selected as the basis for implementation. Agricultural machinery testing platform CloudViewer is adopted to measure index parameters.

B. Analysis of experimental results

To analyze the accuracy of the reconstruction point cloud data, the reconstruction data in Fig. 5 were measured. Randomly chosen 10 groups of reconstrution measurement values compared with manual measurement values. The comparison results are shown in Table III. The mean values of the reconstruction measurement values and manual measurement values are listed in Table IV, take the setting values of trenching machine as the standard values, and calculate the deviation between the mean values and the standard values.

Table IV showed that the accuracy of measuring the reconstructed trench was higher than that of manual measurement. Compared with the artificial mean, the mean of reconstructed trench surface width was increased by 0.31 cm (22.96%), and the mean of trench bottom width and trench depth were also increased by 0.325 cm (28.26%) and 0.47 cm (29.37%), respectively. The data acquisition time was also reduced by 15 $\sim$ 20 minutes. In general, the data measurement accuracy and acquisition efficiency after reconstruction are improved by 22.96% $\sim$ 29.37% and 50% $\sim$ 66.67%, and the accuracy of the measurement results met the requirements of the identification outline (within ± 3 cm).

The measurement error after reconstruction, on the one hand, was caused by the accuracy of 3D LiDAR, and on the other hand, may be caused by normal deviation point matching and Poisson reconstruction algorithm. In the future, we will optimize the point cloud collocation algorithm and surface reconstruction algorithm, measure more experimental data, and optimize the measurement algorithm to compensate the measurement error.

IV. CONCLUSION

We aimed at the requirements of intelligent development of agricultural machinery appraisal, developed a point cloud data acquisition equipment for UAV-LiDAR, proposed a non-contact detection of trench quality, and realized the measurement of trench width, bottom width and depth. Compared with manual measurement, non-contact detection has higher accuracy and faster measurement speed. Therefore, UAV-LiDAR can be used in the dectection of outdoor agricultural machinery to measure the three-dimensional parameters of the target with the developed method, and it is also effective for other types of agricultural machinery.

In a word, the method proposed in this paper not only filled the gap of agricultural machinery intelligent identification, but also successfully applied modern information technology to agriculture and enhanced the modernization level of agricultural dectection. It was conducive to building a comprehensive testing platform for agricultural machinery.

ACKNOWLEDGMENT

This study was funded by Jiangsu Agricultural Science and Technology Innovation and Promotion Fund (Agricultural Machinery New Equipment and New Technology RESEARCH and Development and Promotion) project, which was jointly

carried out by Jiangsu Agricultural Machinery Testing and Identification Station and Nanjing Agricultural University (Project Number: NJ2019-25). Related identification indicators are from the agricultural machinery extension identification outline (No. DG/T 089-2019).

REFERENCES

[1] S. Senthilgavaskar, K. Karthick, and C. Bibin. A review paper on solar operated ridge and furrow formation machine. Materials Today: Proceedings, 46(2), 2021.

[2] C. Yun, H. J. Kim, C. W. Jeon, M. Gang, W. S. Lee, and J. G. Han. Stereovisionbased ridge-furrow detection and tracking for auto-guided cultivator. Computers and Electronics in Agriculture;191:106490–, 2021.

[3] M. A. Matin, J. M. Fielke, and Jma Desbiolles. Torque and energy characteristics for strip-tillage cultivation when cutting furrows using three designs of rotary blade. Biosystems Engineering, 129:329–340, 2015.

[4] Y. Wang, W. Xue, Y. Ma, J. Tong, and J. Sun. Dem and soil bin study on a biomimetic disc furrow opener. Computers and Electronics in Agriculture; 156:209–216, 2019.

[5] C. Yun, H. J. Kim, C. W. Jeon, and J. H. Kim. Stereovision-based guidance line detection method for auto-guidance system on furrow irrigated fields. IFACPapersOnLine; 51(17):157–161, 2018.

[6] J. Roelens, Bernhard Hoefle, S. Dondeyne, J Van Orshoven, and J. Diels. Drainage ditch extraction from airborne lidar point clouds. ISPRS Journal of Photogrammetry and Remote Sensing; 146(DEC.):409–420, 2018.

[7] Yue Pan, Yu Han, Lin Wang, Jian Chen, Hao Meng, Guangqi Wang, Zichao Zhang, Shubo Wang. 3D Reconstruction of Ground Crops Based on Airborne LiDAR Technology. IFAC-PapersOnLine, 52:35-40, 2019.

[8] Guillaume Coiffier, Justine Basselin, Nicolas Ray, Dmitry Sokolov. Parametric Surface Fitting on Airborne Lidar Point Clouds for Building Reconstruction. Computer-Aided Design, 140:103090, 2021.

[9] M. Chakraborty, L. R. Khot, S. Sankaran, and P. W. Jacoby. Evaluation of mobile 3d light detection and ranging based canopy mapping system for tree fruit crops.Evaluation of mobile 3d light detection and ranging based canopy mapping system for tree fruit crops. Computers and Electronics in Agriculture; 158:284–293, 2019.

[10] Yuhan Ji, Shichao Li, Cheng Peng, Hongzhen Xu, Ruyue Cao, and Man Zhang. Obstacle detection and recognition in farmland based on fusion point cloud data. Computers and Electronics in Agriculture; 189:106409, 2021. ISSN 0168-1699.

[11] Zachary S. Brecheisen, Daniel deB. Richter. Gully-erosion estimation and terrain reconstruction using analyses of microtopographic roughness and LiDAR. CATENA, 202:105264, 2021.

[12] C. Fotsing, N. F. Menadjou, and C. Bobda. Iterative closest point for accurate plane detection in unorganized point clouds. Automation in Construction; 125(103610), 2021.

[13] ZHIPENG CAI, TAT-JUN CHIN, ALVARO PARRA BUSTOS, et al. Practical optimal registration of terrestrial LiDAR scan pairs. ISPRS journal of photogrammetry and remote sensing, 2019,147(Jan.):118-131.

[14] Jian Liu, Di Bai, and Li Chen. 3-d point cloud registration algorithm based on greedy projection triangulation. Applied Sciences; 8(10):1776, 2018.

[15] C. Ulas and H. Temeltas. A 3d scan matching method based on multi-layered normal distribution transform. Ifac Proceedings Volumes; 44(1):11602–11607, 2011.

[16] A Xs, A Jp, B Jl, A Py, and A Hg. The iterative closest point registration algorithm based on the normal distribution transformation - sciencedirect. Procedia Computer Science; 147:181–190, 2019.

[17] F. A. Donoso, K. J. Austin, and P. R. Mcaree. Three new iterative closest point variantmethods that improve scan matching for surface mining terrain. Robotics and Autonomous Systems; 2017

[18] H. Hoppe, T. Derose, T. Duchamp, J. Mcdonald, and W. Stuetzle. Surface reconstruction from unorganized points. ACM SIGGRAPH Computer Graphics; 26(2):71–78, 1992.

[19] Y. Ohtake, A. G. Belyaev, M. Alexa, G. Turk, and H. P. Seidel. Multi-level partition of unity implicits. ACM Transactions on Graphics (TOG); 2003.

[20] Peng Wu, Wei Li, Ming Yan. 3D scene reconstruction based on improved ICP algorithm. Microprocessors and Microsystems, 75:103064, 2020.

[21] Cristina Serazio, Marco Tamburini, Francesca Verga, Stefano Berrone. Geological surface reconstruction from 3D point clouds. MethodsX, 8:101398, 2021.

[22] Jules Morel, Alexandra Bac, and Cédric Véga. Surface reconstruction of incomplete datasets: A novel poisson surface approach based on csrbf. Computers Graphics, 74:44–55, 2018.